

Supplementary Information

Supplementary Methods

All stem cell experiments, methods, and protocols for this study were approved by the Stanford University Stem Cell Research Oversight (SCRO) committee. Below is a detailed description of methods and design used in our experiments.

Microfluidic Device Fabrication

Fig. S4 illustrates the fabrication process and shows a completed device. Microfluidic devices consist of a PDMS chip containing microfluidic channels³ bonded on top of a glass slide which features platinum electrodes and a Si₃N₄ passivation layer. All microfabrication was carried out in the UC Berkeley Marvell Nanofabrication Laboratory and the UC Berkeley Biomolecular Nanotechnology Center. Glass slides (Fisher 12-550C) were cut to 50 x 50 mm using a handheld glass cutter and cleaned for 10 min in a Piranha bath at 120⁰ C (1:5 H₂O₂:H₂SO₄). Shipley S1818 photoresist (PR) was spun onto the slides at 4000 RPM for 35 s, leaving a ~2 μm film. PR was soft baked for 5 min on a 90⁰ C hot plate. PR was then exposed on a contact mask aligner (Quintel Q4000) at 175 mJ/cm² (g-line) and subsequently developed in 1:1 MicroDev:H₂O for 35 s, rinsed with DI water and dried with N₂. The substrate was descummed in an O₂ plasma chamber at 50 W for 1 min to improve metal adhesion. 10 nm of Ti followed by 100 nm of Pt were evaporated in an e-beam evaporator, both at 0.1 nm/s (Edwards 306 E-Beam System). Film thickness was continuously monitored using a crystal monitor during deposition. Sheet resistance of metal film was measured at ~ 4 Ω/square using a four-

point resistivity probe. Liftoff was performed by sonicating substrates in acetone for 10 min using a fluoropolymer stand which kept them upright to avoid metal redeposition onto the glass. Remaining PR residue was wiped clean with an acetone soaked tissue, and slides were rinsed with isopropanol and DI water and then blown dry with N₂. Metal film was inspected for pinholes under transmission brightfield microscopy. Next, 400 nm of Si₃N₄ was deposited using plasma-enhanced chemical vapor deposition (PECVD) with 200 sccm NH₃, 200 sccm Ar, 40 sccm SiH₄, 25 W RF plasma, at 900 mTorr chamber pressure and 350⁰ C substrate temperature (Oxford Instruments PlasmaLab 80 Plus). PR was again spin coated, patterned, developed, and descumed as before to define the electrodes and contact pads. The Si₃N₄ was etched using SF₆ reactive ion etching (RIE) at 200 W for 4 min, using 15 sccm SF₆ and 5 sccm O₂, with a 290 mTorr chamber pressure (Reactive Ion Etching System, Plasma Equipment Technology Services). PR was stripped in acetone and the substrates were again cleaned with isopropanol and DI water. Single-layer SU8/silicon molds were prepared using established methods and subsequently treated with Trichloro(1H,1H,2H,2H-perfluorooctyl)silane (Sigma MKBC9893) vapor in a desiccator chamber for >2 hr to provide a non-stick coating.

Polydimethylsiloxane (PDMS, Sylgard 184) was prepared with 1:10 w/w ratio of curing agent to prepolymer, thoroughly mixed, centrifuged to remove bubbles, and poured onto SU8/silicon molds at a thickness of ~5mm. Following desiccation to completely remove bubbles (generally 1-2 hr under house vacuum), the PDMS was oven cured at 60⁰ C for >2 hr and then peeled from the mold. Access holes were punched through the PDMS. Finally, the PDMS and electrode/glass substrate were simultaneously exposed to O₂ plasma at 100 W for 15 s to prepare the surfaces for covalent bonding. To

align the PDMS to the electrodes, two small pieces of scotch tape were attached to the edges of the PDMS to provide a thin spacer, and the device was manually aligned to alignment marks on the substrate under a stereoscope. The PDMS was then pushed down, initiating bonding to the glass, and the tape was removed. The bonded devices were baked at 60⁰ C for >20 min. Detection electrodes were platinized to reduce their impedance⁴ by flowing a solution of chloroplatinic acid (1.4% v/v) and lead acetate (0.02% w/v) in deionized (DI) water through the device and applying a -1.6V DC potential to each 20 μm electrode (vs. Pt reference) for 30 s.

Experimental Procedure

For this study, iPSC-CM clusters were identified under a microscope and scraped from their culture well using a finely drawn sterile Pasteur pipette (see **Movie 3** for example clusters in culture). Some clusters were visibly contracting and others were not. These were allowed to incubate in non-attachment plates for 1 hr, causing them to round up prior to experiments. Clusters were drawn into a syringe, along with a small volume of culture medium. The syringe was connected to the inlet of the device and pushed either by hand or by using a syringe pump automated with the LabVIEW controller software. The cell detection/stimulation/identification protocol is specified as a script which is loaded into the LabVIEW controller. For cell cytometry experiments, the syringe pump was run at 1500 μl/h and the impedance of the detection electrodes was monitored at 100 kHz, 100 mV. A resistance increase of 10 % indicated the presence of a cluster, at which point the flow was stopped and the cluster came immediately to a stop (due to the low Reynolds number, the inertial forces are insignificant). A stimulus pulse sequence of ten

400 μ s current pulses at a 100 ms interval and with current amplitudes of 0.4 – 2.0 mA was administered. The contaminating stimulus artifact was then removed as described above. The processed signal was analyzed for FPs using a thresholding algorithm. Putative FPs which were wider than 1 ms were determined to be authentic. For electrophysiological characterization experiments, cells were positioned over the detection electrodes and the flow was stopped. A battery of stimulus pulse conditions, specified as a script, was loaded into the LabVIEW software and each cluster was stimulated according to the same protocol. This data was then analyzed for trends to explore the stimulus-response parameter space. Cells could be repeatedly stimulated for several hours with no apparent degradation in signal strength or mechanical contractions, indicating cell viability throughout the duration of the cytometry experiments..

Stem Cell Culture

Human induced pluripotent stem cells (iPSC) (iPS(IMR90) line, WiCell, Madison, WI) were maintained in the pluripotent state in 6-well tissue culture plates through daily feeding (2 mL/well) with mTeSR1 media (StemCell Technologies, Vancouver, Canada) supplemented with 1x penicillin/streptomycin (Invitrogen, #15140-163, Carlsbad, CA). Cells were passaged approximately every 4-6 days, at the time when colonies had expanded enough to begin merging with one another. Prior to passaging, new wells were coated with hESC/iPSC-qualified Matrigel (BD Biosciences, #354277, San Jose, CA) diluted in DMEM (Invitrogen, #10569, Carlsbad, CA) and allowed to incubate at room temperature for at least one hour. Cells were removed from their plates mechanically using a scraping tool (Corning, # 3008, Lowell, MA) while still in mTeSR1

from the previous day. The subsequently created cell-media mixture was triturated up and down and was then transferred to each new well of a Matrigel pre-coated 6-well tissue culture plate. Cells were allowed to incubate at 37 °C overnight to promote attachment. The remaining cells not transferred to a new plate were then re-suspended in 90% Knockout Serum Replacement (KOSR) (Invitrogen, #10828010, Carlsbad, CA) with 10% DMSO (Sigma-Aldrich, # D2438, St. Louis, MO) and frozen at -80 °C overnight and then subsequently transferred to liquid nitrogen storage.

Cardiomyocyte Differentiation

Cardiomyocyte differentiation was usually begun 2-5 days after initially seeding iPSC on Matrigel (BD Biosciences). At this time, the cells were transferred to RPMI-1640 media supplemented with B27, 1x non-essential amino acids, 1x penicillin/streptomycin, and 0.1 mM β -mercaptoethanol (all Invitrogen) and our differentiation method was begun using aspects of other methods previously described⁵⁻⁶. On the first day (Day 0) of differentiation, RPMI media with 50 ng/mL of Activin A (R&D Systems, Minneapolis, MN) was added to each well. On the subsequent day (Day 1), 5 ng/mL of BMP-4 (R&D Systems) was added to each well. On Day 3, fresh RPMI media was added to each well and was replaced every 48 hours until Day 11, when the cells were transferred to a DMEM (Invitrogen) media supplemented with 5% FBS (Invitrogen), 1x non-essential amino acids, 1x penicillin/streptomycin, and 0.1 mM β -mercaptoethanol. This DMEM media was then replaced approximately every 48 hours. Cardiomyocytes generally began spontaneously beating sometime between days 9 and

20. A cardiomyocyte cluster positive for the cardiomyocyte marker Troponin-I (TnI) is shown in **Fig. S7**.

Undifferentiated iPSC Embryoid Body Formation

To create clusters, undifferentiated iPSC cells were scraped from culture dishes and triturated as during normal passaging. The cell suspension was then transferred to a 12-well ultra-low-attachment culture plate at 100 μL per well. 1 mL of fresh mTeSR1 was then added to each well. Experiments with resulting clusters were carried out within 2 days.

FEM Modeling of Hydrodynamic Focusing and Flow Switching

In the FEM simulation shown in **Fig. S8**, we examined the minimum entry/exit length for effective hydrodynamic focusing in the channel. To ensure that cells are always positioned over the central electrode, it's important that the flow be fully developed with a sufficiently narrow focusing width, and it is important that this flow not deviate substantially as different outlet valves are opened. In this simulation, we assume the worst case—the outlet furthest from the centerline is selected. We prescribe a total channel width of 400 μm , or ~ 40 cell radii (cell radii = 10 μm), a channel height of 100 μm , and a total channel length of 1000 μm . With a cell suspension flow rate, Q_c , of 6.0 nL/s and a sheath flow rate, Q_s , of 18 nL/s, we can focus (single) cells to within ± 3 cell radii of the centerline ($W_{\text{focus}} \sim \pm 30 \mu\text{m}$), which is adequate for single cell and cluster FP detection. At these flow rates, we have an average cell velocity of 1 mm/s through the channel, which is what we have used in our experiments. From this model, L_{exit} was

observed to be $\sim W_{chan}$, or 400 μm , and L_{entry} was observed to be $\sim W_{inlets}$, or 150 μm .

Provided that the electrode detection region is placed sufficiently far from the entry/exit regions, cells will always flow over the central detection electrode, regardless of which outlet is open.

COMSOL Multiphysics 3.4 was used for this analysis in the Incompressible Navier-Stokes fluid mechanics mode. The fluid density and viscosity were assumed to be 1000 kg/m^3 and 0.001 $\text{Pa}\cdot\text{s}$, respectively. No-slip boundary conditions were applied to the channel walls, laminar inlet flow rate boundary conditions were set at the cell/sheath inlets, and the selected outlet boundary was set to a constant pressure boundary condition.

FEM Modeling of Field Potential in Microchannels

Fig. S9 shows a COMSOL Multiphysics 3.4 model showing that extracellular voltage increases as cross-sectional channel area decreases. In these DC simulations, we are modeling a 10 μm sphere with inward current density of 1 mA/cm^2 , which is a reasonable Na^+ current density. As this is an estimate of the maximum current magnitude during excitation, the FPs calculated would represent the maximum (negative) deflection. The electrode is assumed to be on the channel floor, directly under the cell. The channel length is 1 mm, and the reference electrode is assumed to be 1mm away. Separating the cell from the electrode does not have a dramatic effect on the FP amplitude. (a) A 10 μm cell confined to a channel that is 3 cell diameters in width and 3 cell diameters in height (30 x 30 μm) will produce a FP amplitude of 204 μV in its immediate vicinity. (b, c) Widening the channel to 200 μm causes the FP to drop to 85.6 μV , and further increasing its height to 100 μm reduces the FP to 69.8 μV . This is also a reasonable representation

for a microelectrode array, where the cells are adhered on the electrode substrate and ions are free to propagate in a (virtually) unrestricted hemisphere around the cell. (d) Finally, with no channel walls, ions propagate radially in all directions around the cell, and the FP drops to $46.7 \mu\text{V}$. Each 2D slice plot shows the extent of the FP, with black = maximum potential deflection and white = 0 V for that particular geometry. Medium conductivity was assumed to be 1 S/m. The FEM plot in **Figure 2d** was generated using the same approach. In modeling the depolarization potential in **Figure 2d**, a $35 \mu\text{m}$ channel height was used with a $20 \mu\text{m}$ diameter cell located $5 \mu\text{m}$ above the channel floor.

FEM Modeling of Field Stimulation in Microchannels

During stimulation, an optoisolated current source injects a controlled current pulse into the channel through large electrodes directly upstream and downstream of the cell. Because the channel is several times longer than it is wide/tall, a uniform current density field oriented normal to the channel cross section results in the vicinity of the cell. As the membrane is predominantly capacitive, its initial impedance following a current step is low. But as the membrane charges up to its steady-state value, the current through the membrane decreases, and the current in the channel is diverted around the cell (**Fig. S11a**). The membrane voltage reaches a steady-state after approximately $1 \mu\text{s}$ (**Fig. S1b**).

In the model shown above and in **Figure 2c**, the same geometry was used as described previously for FP simulation. A $50 \mu\text{A}$ stimulus current pulse was applied between two $30 \times 100 \mu\text{m}$ stimulus electrodes on the floor of the channel spaced $45 \mu\text{m}$ apart. Conductivity of the channel, cell membrane, and cytoplasm were assumed to be 1.6 S/m, 0.1 mS/m, and 0.25 S/m, respectively. Relative permittivity of the channel, cell

membrane, and cytoplasm were assumed to be 78, 8, and 50, respectively. A transient electric current simulation was developed in COMSOL Multiphysics 3.4. Slice plots were rendered at $t = 1 \mu\text{s}$ after the current step was applied, at which point the transmembrane voltage has reached steady state.

Physics of Field Potential Signals and Relationship to Transmembrane Action Potential

The FP is the ohmic potential drop in the resistive medium surrounding a cell arising from transmembrane ion currents. Transient changes in membrane permeability during excitation lead to various diffusive ion currents (primarily, Na^+ , K^+ , and Ca^{2+}) in and out of the cell. These permeability changes also cause characteristic shifts in the Goldman-Hodgkin-Katz potential across the cell membrane, giving rise to the so-called transmembrane action potential signal. **Fig. S12** illustrates the computation of the FP due to the transmembrane current density. Electrically, the transmembrane current density can be regarded as a capacitive charging current due to the changes in the Goldman-Hodgkin-Katz potential:

$$J_m = C_m \frac{dV_m}{dt}$$

where C_m is the specific capacitance of the cell membrane. The differential voltage, dV , across a spherical shell around the cell with resistance dR , is:

$$dV = I_m \cdot dR = 4\pi r_{cell}^2 J_m \cdot dR$$

where r_{cell} is the radius of the cell. Integrating this between two electrodes, one close to the cell and one far from the cell:

$$\begin{aligned} V_{FP} &= 4\pi r_{cell}^2 J_m \int_{r_{close}}^{r_{far}} \frac{1}{\sigma} \left(\frac{r_{cell}}{r_{far}} - \frac{r_{cell}}{r_{close}} \right) \\ &= \frac{J_m r_{cell}}{\sigma} \left(\frac{r_{cell}}{r_{far}} - \frac{r_{cell}}{r_{close}} \right) \end{aligned}$$

where σ is the conductivity of the medium. Therefore, the FP is related to the more familiar action potential (V_m) by:

$$V_{FP} = \frac{C_m r_{cell}}{\sigma} \left(\frac{r_{cell}}{r_{far}} - \frac{r_{cell}}{r_{close}} \right) \frac{dV_m}{dt}$$

To maximize this signal, we need $r_{far} \gg r_{cell}$ and $r_{close} \ll r_{cell}$. FP recordings are often thought of as imprecise when compared with action potential signals because SNR is weaker and the geometries of the electrodes and current distributions cannot be precisely controlled in conventional microelectrode arrays. In our device, cell positioning is quite repeatable and electrode spacing is fixed. Furthermore, microchannels enhance the FP signal by confining the current distribution to a smaller volume (rather than an infinite sphere, as considered here). For these reasons, we expect our system to produce quantitative electrophysiological parameters from cells using FP signals.

Supplemental References

1. US Patent #2656508, Means for counting particles suspended in a fluid, W.H. Coulter (1953)
2. McGill, K.C. et al. On the Nature and Elimination of Stimulus Artifact in Nerve Signals Evoked and Recorded Using Surface Electrodes. *Biomedical Engineering, IEEE Transactions on BME-29*, 129-137 (1982).
3. Duffy, D.C., McDonald, J.C., Schueller, O.J.A. & Whitesides, G.M. Rapid Prototyping of Microfluidic Systems in Poly(dimethylsiloxane). *Analytical Chemistry* **70**, 4974-4984 (1998).
4. Malleo, D. et al. Note: Characterization of electrode materials for dielectric spectroscopy. *Rev. Sci. Instrum.* **81**, 016104 (2010).
5. Laflamme, M.A. et al. Cardiomyocytes derived from human embryonic stem cells in pro-survival factors enhance function of infarcted rat hearts. *Nat Biotech* **25**, 1015-1024 (2007).
6. Yang, L. et al. Human cardiovascular progenitor cells develop from a KDR+ embryonic-stem-cell-derived population. *Nature* **453**, 524-528 (2008).
7. Marcus, J.S., Anderson, W.F. & Quake, S.R. Microfluidic Single-Cell mRNA Isolation and Analysis. *Anal. Chem.* **78**, 3084-3089 (2006).
8. Thorsen, T., Maerkl, S.J. & Quake, S.R. Microfluidic Large-Scale Integration. *Science* **298**, 580-584 (2002).
9. Unger, M.A., Chou, H.-P., Thorsen, T., Scherer, A. & Quake, S.R. Monolithic Microfabricated Valves and Pumps by Multilayer Soft Lithography. *Science* **288**, 113-116 (2000).

10. Bansal, T., Chang, M.-P. & Maharbiz, M.M. A class of low voltage, elastomer-metal “wet” actuators for use in high-density microfluidics. *Lab Chip* **7**, 164-166 (2007).
11. Kattman, S.J., *et al.* Stage-Specific Optimization of Activin/Nodal and BMP Signaling Promotes Cardiac Differentiation of Mouse and Human Pluripotent Stem Cell Lines. *Cell Stem Cell* **8**, 228-240 (2011).
12. Burridge, P.W., *et al.* A Universal System for Highly Efficient Cardiac Differentiation of Human Induced Pluripotent Stem Cells That Eliminates Interline Variability. *PLoS ONE* **6**, e18293 (2011).

Supplementary Figures

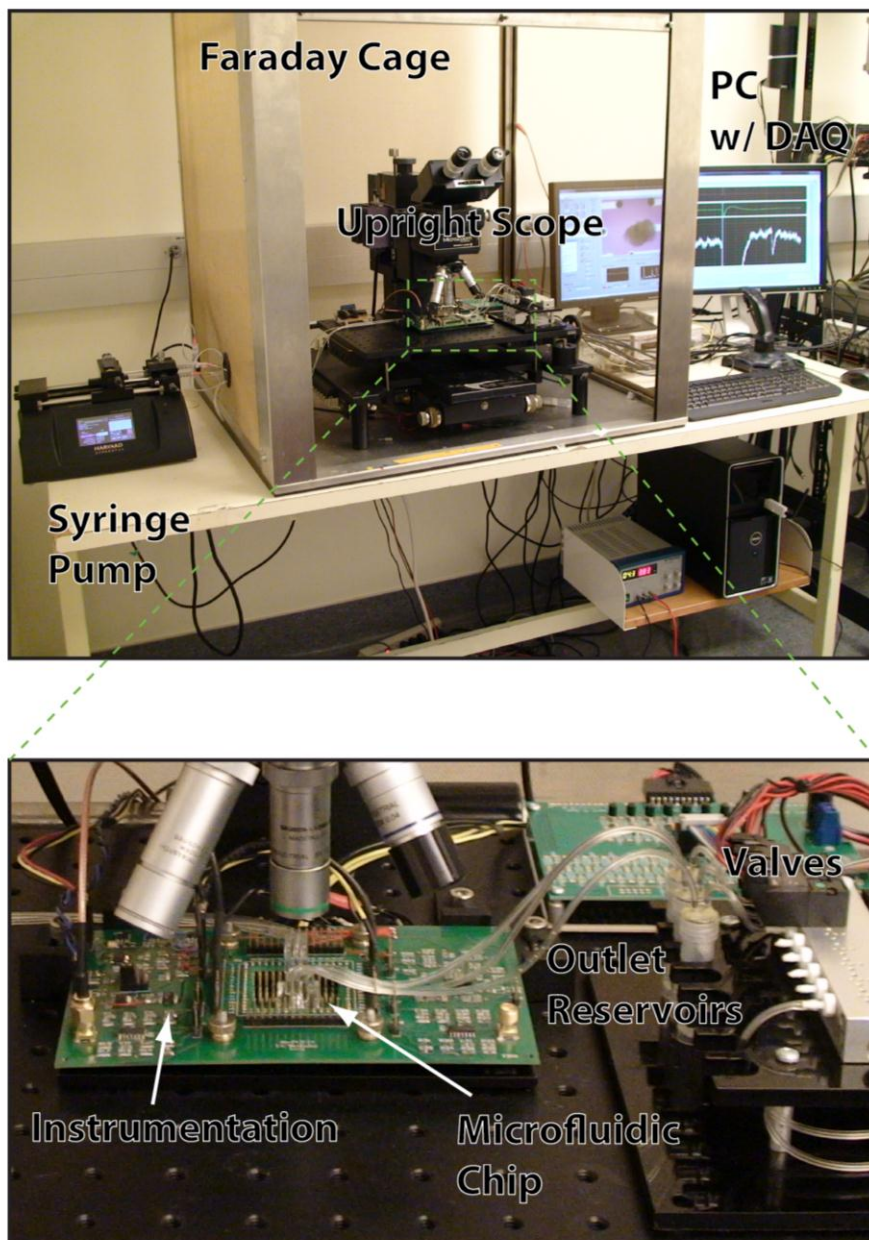


Fig. S1. EPACC instrumentation.

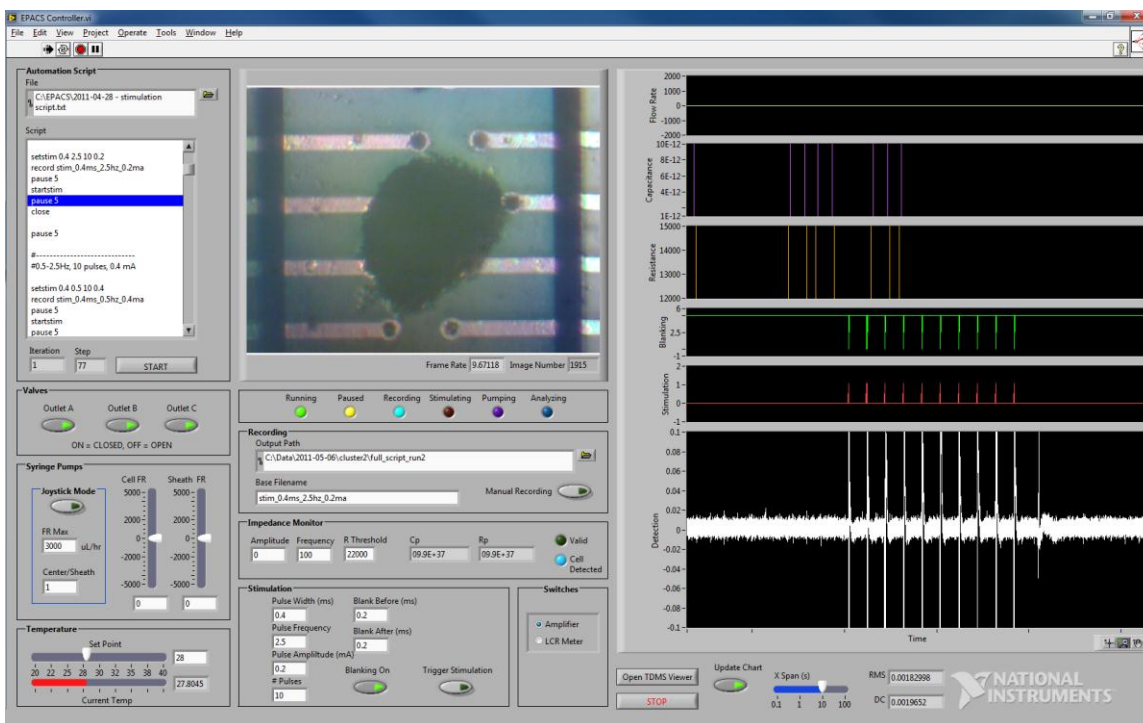


Fig. S2. A screenshot of our custom LabVIEW controller, which includes syringe pump control for both the cell suspension and sheath flow, impedance-based cell detection, stimulation control, recording of FP signals, artifact elimination, outlet valve actuation, temperature control, and video recording.

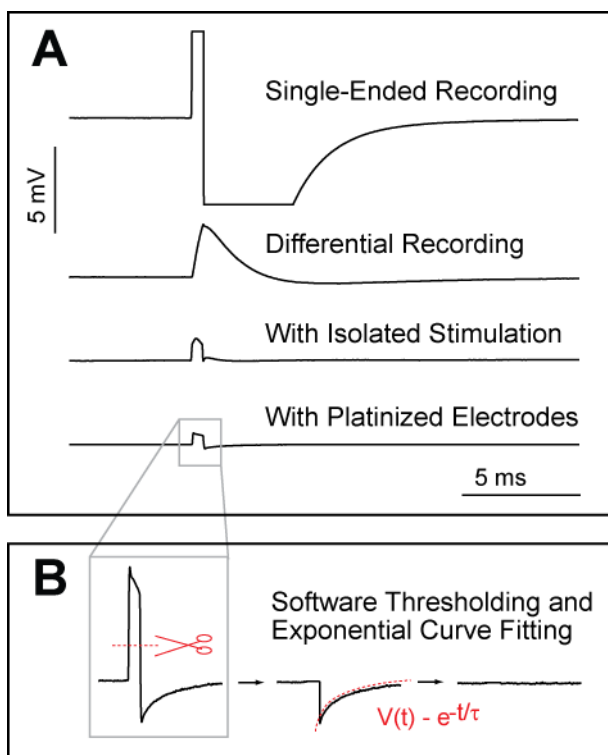


Fig. S3. (a) Stimulus artifact suppression. In these experiments, a 100 μA , 500 μs pulse was delivered and the resulting artifact was observed. Single-ended recordings, in which one electrode was recorded with respect to a single-ended on-chip Pt reference electrode, caused amplifier saturation for 4 ms. Differential recording between the two detection electrodes dramatically reduces this artifact and eliminates amplifier saturation. When using an optoisolated stimulator, the recovery time drops significantly since the stimulus charge does not discharge through the recording amplifier. Finally, platinizing electrodes further reduces artifact. (b) The remaining artifact can be eliminated in software by blanking samples during stimulation and fitting the remaining RC decay to an exponential decay function, which is subsequently subtracted out.

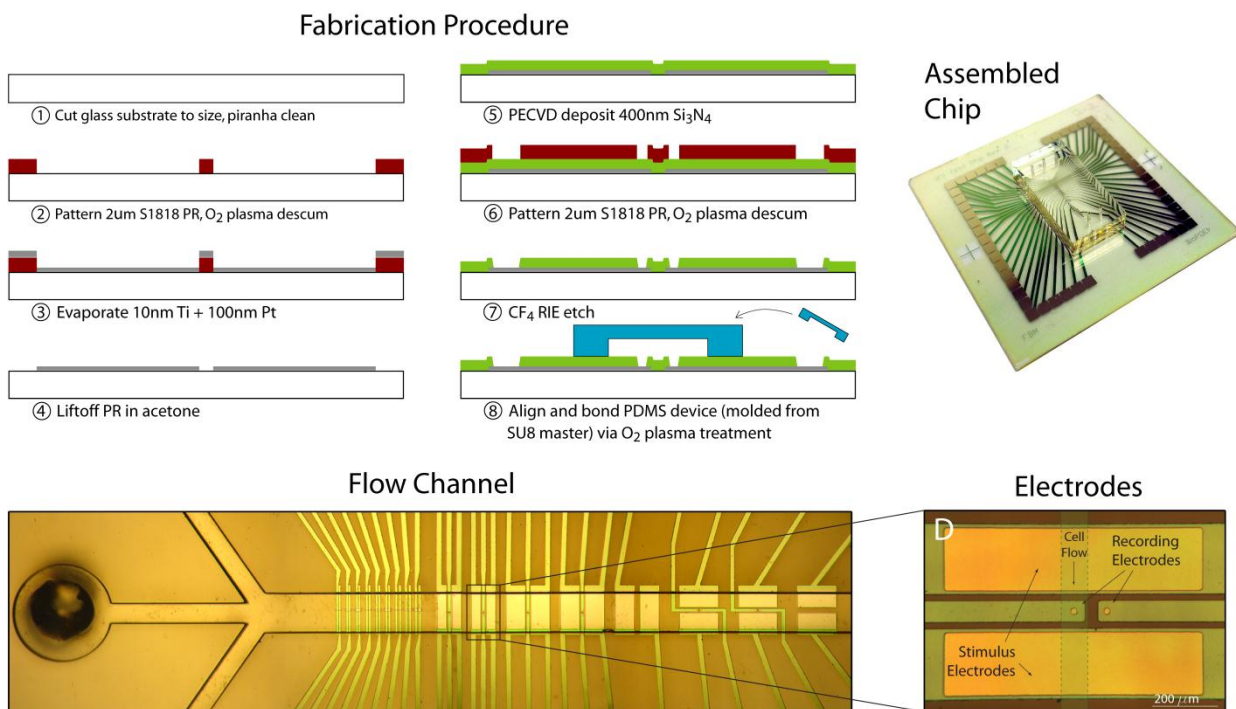


Fig. S4. Outline of the microdevice fabrication procedure, including metal deposition, metal liftoff, silicon nitride deposition, silicon nitride etching, and PDMS bonding. Bottom images show the flow channel, with a close-up view of the electrodes (rotated by 90°), taken with an upright microscope. An assembled chip is shown at the top right.

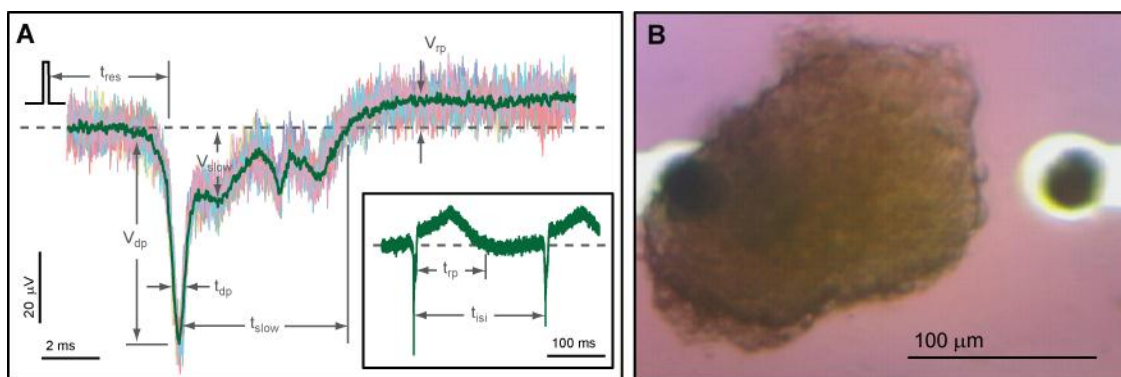


Fig. S5. (a) Spontaneous FPs averaged 10X to reduce noise. Many features of the FP can be observed: response time (t_{res}), depolarization time (t_{dp}), slow current time (t_{slow}), repolarization time (t_{rp}), interspike interval (t_{isi}), depolarization amplitude (V_{dp}), slow current amplitude (V_{slow}), and repolarization amplitude (V_{rp}). Inset shows two successive spontaneous FPs. The significance of these features is explored in (14). (b) An iPSC-CM cluster positioned over one detection electrode, with the differential reference electrode on the right.

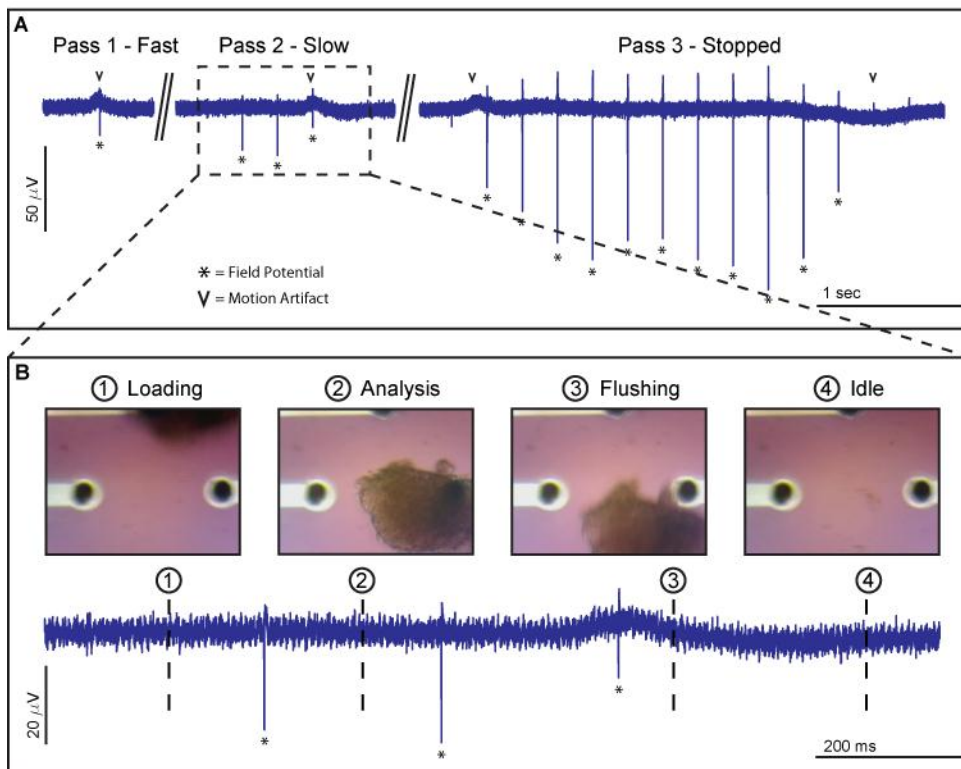


Fig. S6. (a) A spontaneously beating iPSC-CM cluster is passed over detection electrodes and the FP is observed when the cluster is moved quickly, slowly, and when it is held stationary over the electrode for 3 seconds. (b) Close-up of the signals observed in the slow case. **Supplementary Movie 2** shows this experiment. Asterisks signify FPs in (a) and (b).

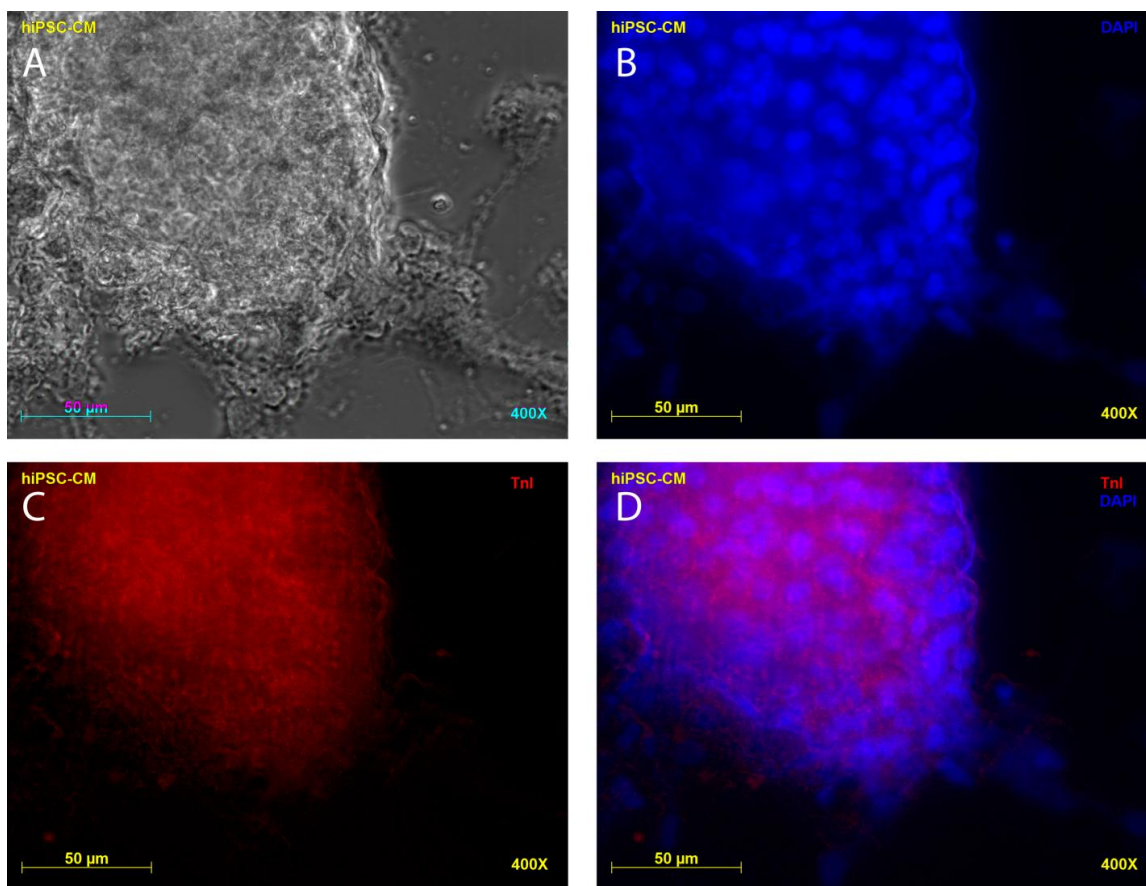


Fig. S7. Immunostaining results indicating that iPSC-derived cardiomyocyte clusters express cardiac Troponin I uniformly throughout the cluster. **(a)** Brightfield image of iPSC-CM cluster. **(b)** DAPI. **(c)** TnI. **(d)** Merged.

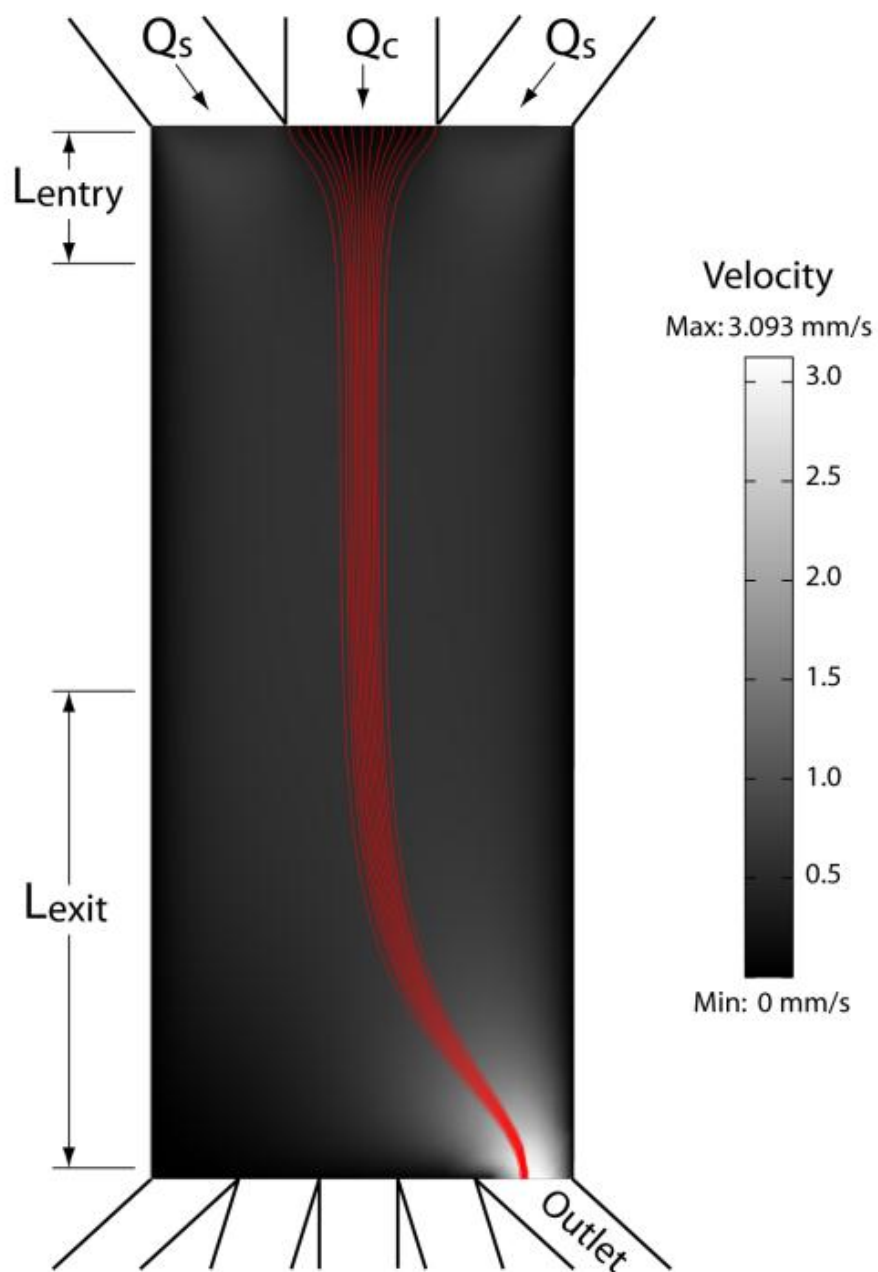


Fig. S8. FEM model of hydrodynamic focusing in a cytometry channel, where the grayscale slice plot indicates velocity and the red streamlines indicate the flow focusing from the center channel. This plot assumes the worst-case streamline deviation (i.e. the

most off-center outlet is selected). The plot shows that the entry length and exit length of the cell stream are roughly equal to the inlet width and channel width, respectively.

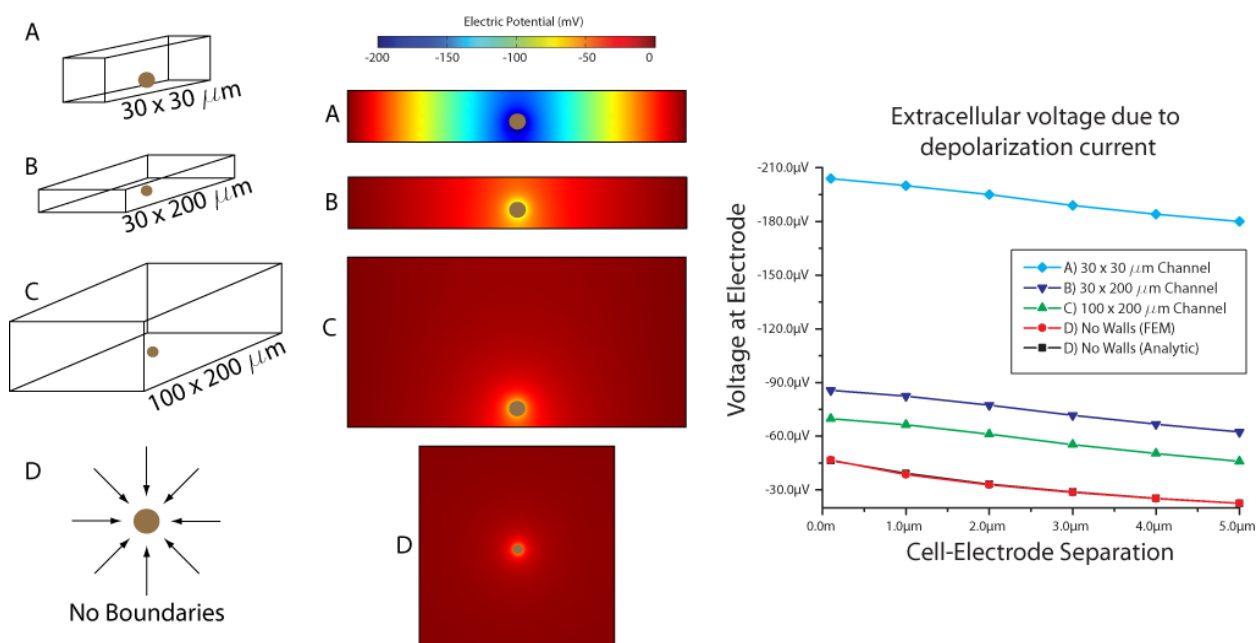


Fig. S9. FEM model showing that microchannels enhance FP amplitudes. **a**, **b**, and **c** represent 30×30 , 30×200 , $100 \times 200 \mu\text{m}$ channels, respectively. **d** represents an infinite boundary, where the lines of current are not confined and are equal in all directions. Extracellular voltage in the vicinity of the cell drops marginally as the cell-electrode separation distance increases (i.e., for non-adhered cells), but the increase in potential attributed to microchannel confinement more than makes up for this drop, indicating that non-adhered cells can be analyzed in microchannels.

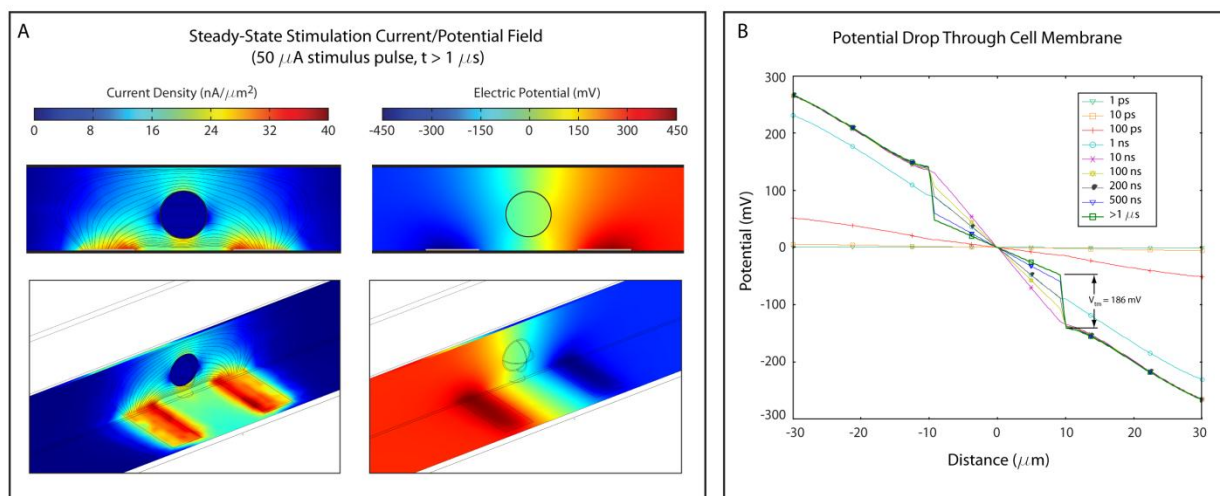


Fig. S10. (a) FEM model showing steady-state current density and potential field for a cell under stimulation by a 50μ A pulse. (b) Line plots at successive time points, showing that steady-state potential drop across the membrane is reached at $t = 1 \mu$ s.

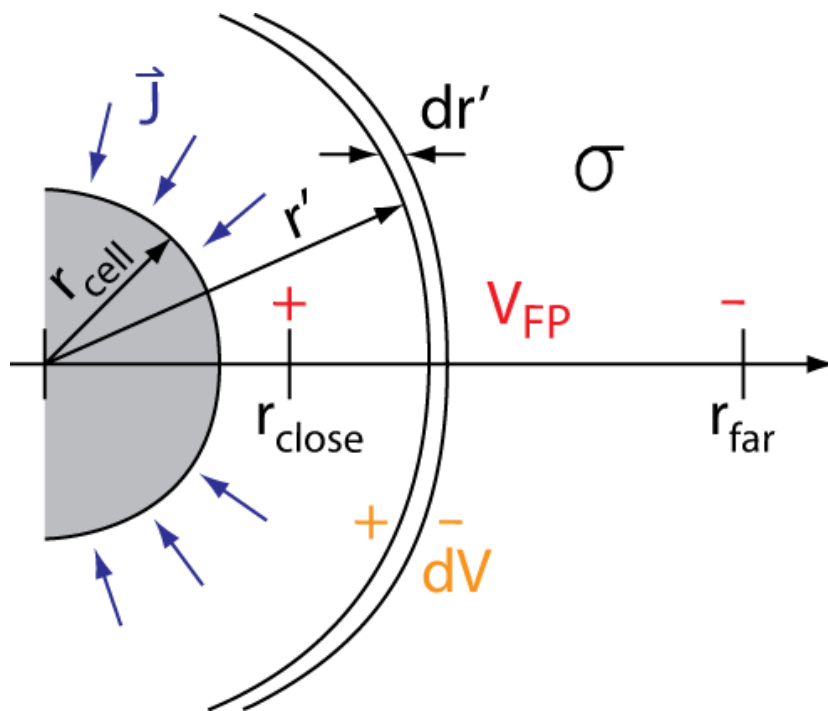


Fig. S11. Illustration of the mathematics behind computing the FP surrounding a depolarizing cell. The differential potential, dV , arising from the ohmic potential drop of the cell's inward current density, J , through the medium with conductivity σ , can be integrated for a spherical shell with elements dr' between radii r_{far} and r_{close} , resulting in the total FP amplitude, V_{FP} .

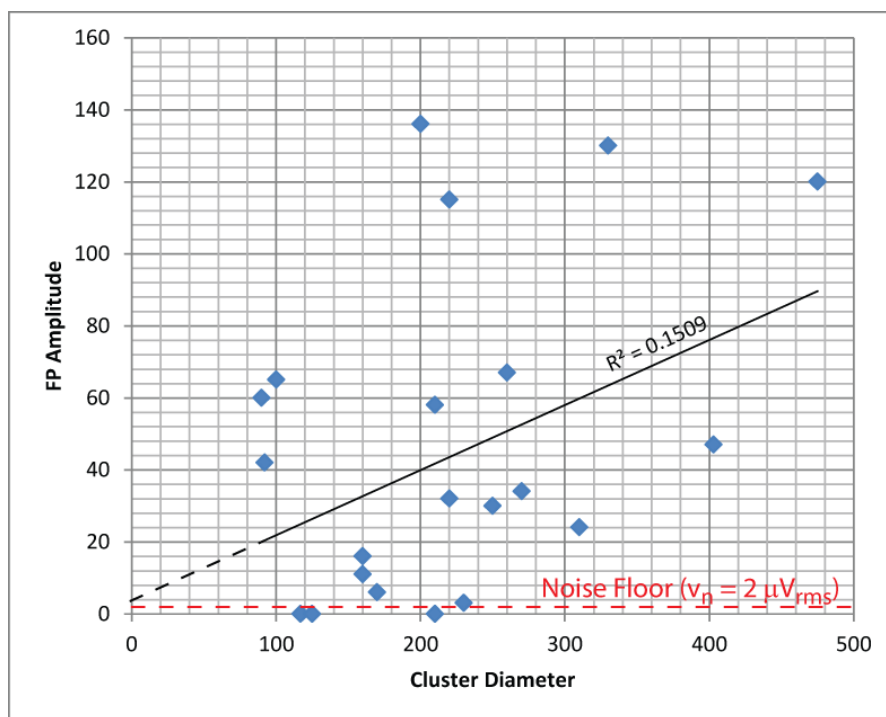


Fig. S12. We have successfully applied EPACC to clusters ranging from 90 – 475 μm, with a mean diameter of 218 μm. To examine if there is a fundamental lower limit to the diameter of cluster which can be detected, we compared the diameter of clusters with their FP amplitudes to determine at what point these amplitudes drop below the noise floor of our detection system. We found a slight correlation ($R^2 = 0.1509$) between cluster diameter and FP amplitude. However, given the wide distribution of amplitudes for any given cluster diameter, it seems that local variations in electrophysiological activity near the electrode may be far more important than the overall cluster size. Given that the trend line is well above the noise floor at the diameters corresponding to a single cell (10 μm), it seems plausible that even single cells could be detected. The difficulty in single cell detection may ultimately lie in positioning cells over electrodes (and possibly employing a trap-and-release scheme to do so), and not in actually performing the signal detection.

Supplementary Movies

Movie 1: Identifying responsive and non-responsive iPSC-CM clusters

This video shows field potential (FP) recordings and system state data for the Electrophysiology-Activated Cell Cytometer (EPACC), first during the analysis of a non-responsive cluster and then during analysis of a responsive cluster which shows both evoked and spontaneous FP signals.

Movie 2: Spontaneously beating cluster in flow

This video shows a spontaneously beating cluster in constant flow over detection electrodes. FPs as well as motion artifacts are clearly visible in the recording.

Movie 3: iPSC-CM clusters in culture dish

This video shows several examples of cell clusters in a culture dish of iPSCs that have undergone our differentiation protocol. Several of these clusters are spontaneously beating whereas others are not. Our cell cytometer is capable of distinguishing (1) clusters which produce spontaneous and evoked FPs, (2) clusters which only produce evoked FPs, and (3) clusters which have no electrophysiological activity.